Transport parameterization of the Polar SWIFT model (version 2)

Ingo Wohltmann[1] and Daniel Kreyling[1]

[1]Alfred Wegener Institute for Polar and Marine Research, Potsdam, Germany

Correspondence: I. Wohltmann (ingo.wohltmann@awi.de)

Abstract. The Polar SWIFT model is a fast scheme for calculating the chemistry of stratospheric ozone depletion in the polar vortex in winter. It is intended for use in General Circulation Models (GCMs) and Earth System Models (ESMs) to enable the simulation of interactions between the ozone layer and climate, when a full stratospheric chemistry scheme is computationally too expensive. Many GCMs do not include a usable general scheme for the transport and mixing of chemical species in the stratosphere. When using the Polar SWIFT model in a GCM, it is usually necessary to parameterize the transport of ozone in order to obtain the total change of ozone as the sum of the change by transport and by chemistry. We present a transport parameterization for the Polar SWIFT model that simulates the change of vortex-averaged ozone by transport in a fast and simple way without the need for a complex transport scheme in the GCM.

1 Introduction

The importance of interactions between climate change and the ozone layer has long been recognized (e.g., Thompson and Solomon, 2002; Rex et al., 2006; Nowack et al., 2015). Hence, it is desirable to account for these interactions in climate models. Since a full stratospheric chemistry scheme is computationally very expensive, several fast schemes for ozone chemistry, like the Cariolle scheme (Cariolle and Déqué, 1986; Cariolle and Teyssèdre, 2007) or Linoz (McLinden et al., 2000; Hsu and Prather, 2009), have been developed. Polar SWIFT has been developed to improve on these schemes for polar ozone chemistry (Wohltmann et al., 2017). So far, Polar SWIFT and the transport parameterization have been implemented into the ECHAM6 climate model (Romanowsky et al., 2019), the AFES4.1 climate model (publication for the AFES version using SWIFT under preparation, for a general description of AFES, see Ohfuchi et al., 2004; Enomoto et al., 2008; Kuwano-Yoshida et al., 2010), and the ICON-NWP model 2.6.3 (publication under preparation, for a general description, see Zängl et al., 2015).

Polar SWIFT simulates the evolution of the polar vortex-averaged mixing ratios of key species that are involved in polar ozone depletion by solving a set of coupled differential equations for these species on a small number of vertical levels (Wohltmann et al., 2017). That is, only a single value is computed per level. The model includes the four prognostic variables $ClONO_2$, HCl, HNO_3, and O_3.

When using the Polar SWIFT model to simulate the ozone chemistry in a GCM, it is usually necessary to parameterize the transport of ozone in order to obtain the total change of ozone as the sum of the change by transport and chemistry. The transport parameterization computes only one vortex-averaged value for the change of ozone by transport per level. Then, the simulated total vortex-averaged change in ozone is the sum of the vortex-averaged change by transport by the transport parameterization

and the vortex-averaged change by chemistry by Polar SWIFT. The transport parameterization includes a "constant change" term that just adds a constant amount of ozone per time step of the model, and a temperature-dependent term that considers the interannual variability in ozone transport caused by interannual variability in the Brewer-Dobson circulation.

30   The transport parameterization is based on a fit to the transport of ozone modelled in the global Lagrangian ATLAS Chemistry and Transport Model (see Wohltmann and Rex, 2009, for a detailed description) for many different winters in the northern and southern hemisphere (Wohltmann et al., 2017). The ATLAS runs use the full transport and mixing scheme of the ATLAS model, while the detailed stratospheric chemistry scheme of the ATLAS model is replaced by the simplified Polar SWIFT model to obtain self-consistent results.

2   Prerequisites

2.1   Definitions

SWIFT and the transport parameterization are based on 5 levels at $69.66111\,\text{hPa}$, $54.03643\,\text{hPa}$, $41.59872\,\text{hPa}$, $31.77399\,\text{hPa}$ and $24.07468\,\text{hPa}$ (rounded values are used in the text the following). In order to derive the parameterization, these levels are extended into adjacent layers centered at the levels. The vortex edge is assumed at $\pm 36\,\text{PVU}$ potential vorticity at $475\,\text{K}$ for the northern and southern hemisphere, respectively. The vortex edge criterion is extended to other altitudes than $475\,\text{K}$ by the modified potential vorticity of Lait (1994).

2.2   Model runs of the ATLAS-SWIFT model

The ATLAS-SWIFT model runs are driven by meteorological data from the European Centre of Medium-Range Weather Forecasts (ECWMF) ERA5 reanalysis (provided on a 1.125° x 1.125° horizontal grid, $3\,\text{h}$ temporal resolution, 137 model levels) (Hersbach et al., 2020). The model uses a hybrid vertical coordinate that is identical to a pure potential temperature coordinate for a pressure lower than $100\,\text{hPa}$. Diabatic heating rates from ERA5 are used to calculate vertical motion. The vertical range of the model domain is $350\text{–}1900\,\text{K}$ and the horizontal resolution of the model is $150\,\text{km}$ (mean distance between air parcels). The runs are set up in a way similar to setup of the runs used in Wohltmann et al. (2017). Polar SWIFT is implemented in ATLAS by adding the rate of change of ozone calculated by Polar SWIFT for a given layer to the ozone value of every air parcel inside the vortex and inside this layer. Note that this means that the ozone field does still vary across the vortex. The same is done for the other simulated species HCl, $ClONO_2$ and HNO_3. The vortex means of these species, which are needed as input at the start of every time step, are obtained by averaging over all air parcels inside the vortex in each layer. Outside of the polar vortex, O_3, Cl_y, HCl, HNO_3 and $ClONO_2$ are reinitialized every day with seasonal climatologies. For O_3 and HNO_3, a seasonal climatology based on all available data of the MLS satellite instrument (e.g., Livesey et al., 2020) is used (i.e., which is a function of the month of year, with data from all years averaged). Cl_y, $ClONO_2$ and HCl are taken from a seasonal climatology derived from ATLAS runs with the full chemistry model. While HCl is available from MLS data, it is not used here so that the sum of HCl and $ClONO_2$ is consistent with Cl_y.

Simulations of the Arctic winters 1979/1980–2020/2021 and the Antarctic winters 1980–2021 are performed. For every winter and hemisphere, a new run is started which is initialized with species mixing ratios from the same MLS and ATLAS climatologies that are used for the reinitialization described above (i.e., the same initial species concentrations in every year). Runs start on 1 November and end on 31 March in the northern hemisphere and start on 1 May and end on 30 November in the southern hemisphere. The long-term change in the chlorine loading of the stratosphere is considered by multiplying the Cl_y, HCl and $ClONO_2$ values by a number obtained by dividing the Equivalent Effective Stratospheric Chlorine (EESC, Newman et al., 2007) of the given year by the EESC of the year 2000.

3 Transport parameterization

The derivation of the transport parameterization is based on vortex averages in a small number of vertical layers to comply with the formulation of the chemistry in the Polar SWIFT model. First, the vortex-averaged total modelled ozone change per day in a layer $\Delta O_{3,\text{total}}$ in the ATLAS-SWIFT runs is separated into the ozone change per day by transport $\Delta O_{3,\text{transport}}$ and the ozone change per day by chemistry $\Delta O_{3,\text{chem}}$:

$$\Delta O_{3,\text{total}} = \Delta O_{3,\text{chem}} + \Delta O_{3,\text{transport}} \tag{1}$$

All quantities are based on ozone volume mixing ratios. The vortex-averaged ozone change by chemistry per day in a layer $\Delta O_{3,\text{chem}}$ is obtained by the rate of change of ozone from the ATLAS-SWIFT model. Throughout any given layer in the vortex, the ozone change by chemistry is constant and is a direct result of the equations of the Polar SWIFT model. The total modelled ozone change per day in a layer $\Delta O_{3,\text{total}}$ is obtained by the difference in the modelled vortex-averaged ozone in a layer between two consecutive days. Finally, the vortex-averaged ozone change by transport per day in a layer $\Delta O_{3,\text{transport}}$ is the difference between the total modelled change and the change in chemistry.

All time series of the vortex-averaged values are limited to include only values when the vortex existed. For each year and hemisphere, a date of "vortex formation" and a date of "vortex breakup" are defined. There is some uncertainty and arbitrariness in these dates, since these are long-term processes, but the sensitivity of the results to the dates chosen is small. For the northern hemisphere, vortex formation is defined as the date when the area of the vortex first exceeds 15 million km^2 at 54 hPa. Vortex breakup is defined as the last date when the area of the vortex was above 15 million km^2 at 54 hPa (but limited to the last date of the model run when the vortex existed longer than March). These values can be found in Table 1. For the southern hemisphere, a "formation" date of 1 May and a "breakup" date of 31 October are assumed for all years.

As an example, Figure 1 shows the cumulated changes obtained in this way for the northern hemispheric winter 2010/2011 and the southern hemispheric winter 2011 at 54 hPa (layer 2) as a function of the day of year. Figures for all years, layers and both hemispheres can be found in a supplement (this applies to all following figures). The total change (Figure 1 a, b) is the sum of the change by chemistry (Figure 1 c, d) and change by transport (Figure 1 e, f). All cumulated time series start with 0 at the vortex formation date. This arbitrary definition will not be of relevance in the following, since constant offsets will always cancel out.
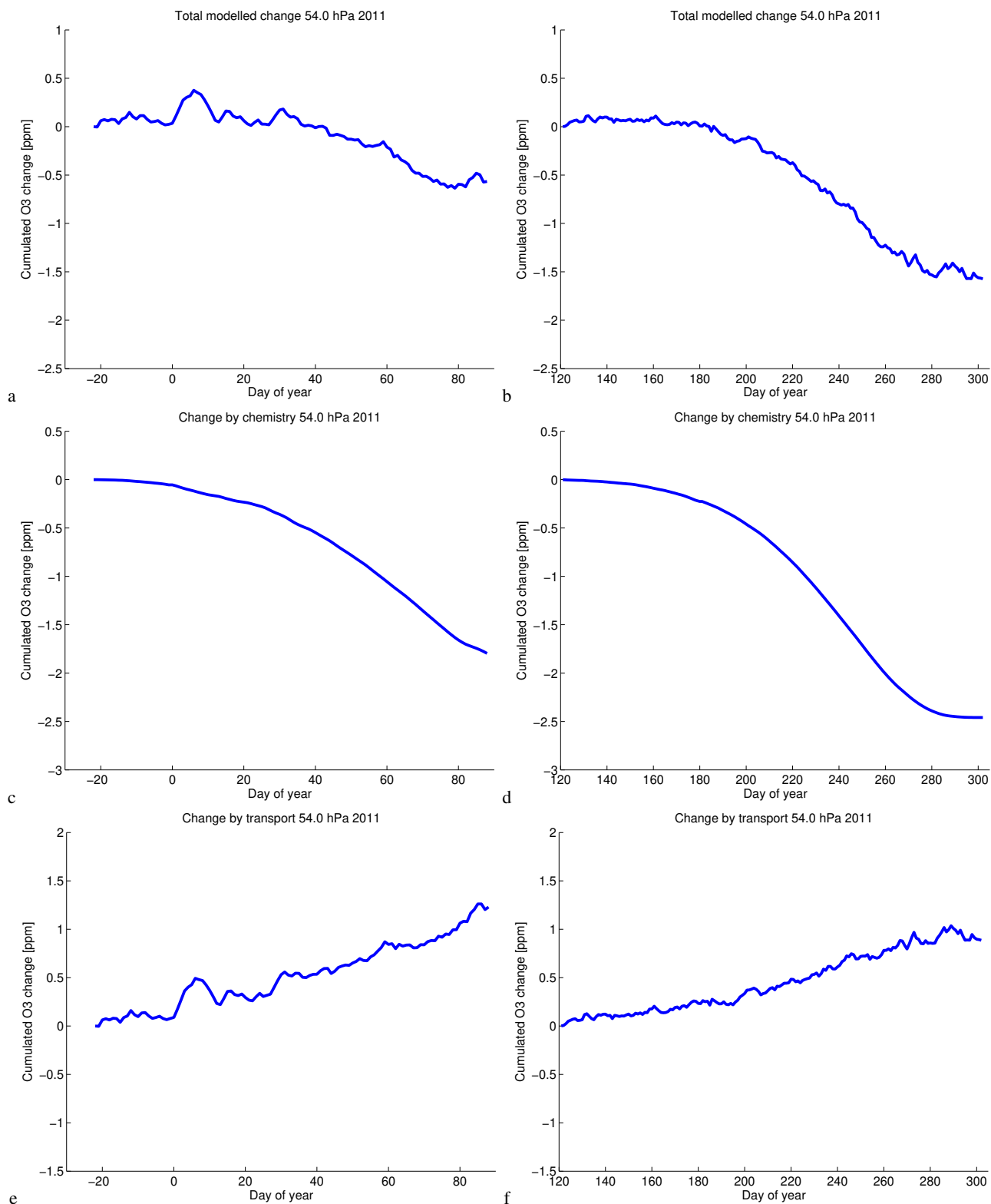
Figure 1. Cumulated change of vortex-averaged ozone mixing ratio for the northern hemispheric winter 2010/2011 (a, c, e) and the southern hemispheric winter 2011 (b, d, f) at 54 hPa simulated by ATLAS-SWIFT as a function of the day of year. Panels (a, b) show the total simulated change, panels (c, d) show the change by chemistry and panels (e, f) show the change by transport.

Table 1. Assumed dates of vortex formation and breakup in the northern hemisphere

Year	Formation	Breakup	Year	Formation	Breakup
1980	29 Dec	14 Mar	2001	26 Jan	18 Feb
1981	9 Dec	15 Feb	2002	15 Dec	16 Feb
1982	12 Dec	26 Mar	2003	8 Dec	20 Mar
1983	27 Nov	10 Mar	2004	14 Dec	22 Jan
1984	4 Dec	5 Mar	2005	20 Dec	24 Mar
1985	7 Dec	18 Jan	2006	2 Jan	28 Jan
1986	21 Dec	21 Mar	2007	10 Dec	10 Mar
1987	30 Nov	31 Jan	2008	24 Dec	1 Mar
1988	24 Jan	23 Mar	2009	18 Dec	5 Feb
1989	10 Dec	7 Mar	2010	6 Jan	21 Feb
1990	5 Dec	30 Mar	2011	10 Dec	30 Mar
1991	26 Nov	2 Feb	2012	2 Dec	5 Feb
1992	7 Dec	29 Mar	2013	10 Dec	24 Jan
1993	3 Dec	22 Mar	2014	11 Dec	30 Mar
1994	12 Dec	31 Mar	2015	13 Dec	25 Mar
1995	6 Dec	29 Mar	2016	30 Nov	11 Mar
1996	6 Dec	30 Mar	2017	4 Jan	27 Feb
1997	17 Jan	30 Mar	2018	19 Dec	22 Feb
1998	17 Dec	28 Feb	2019	2 Dec	1 Mar
1999	9 Dec	1 Jan	2020	12 Dec	30 Mar
2000	16 Dec	18 Mar	2021	9 Dec	7 Feb

3.1 "Constant change" term

Figure 2 shows the cumulated vortex-averaged ozone change by transport at 54 hPa (layer 2) for the northern hemispheric winter 2010/2011 and the southern hemispheric winter 2011 (blue) again. The change as a function of time is linear to a good approximation in both winters. It turns out that this also is a good approximation for all other years and layers (see supplement). This suggests an approach where a constant amount of ozone is added in each layer per time step of the SWIFT model.

A linear regression line is fitted to the cumulated change for each year (red). For the parameterization, the slopes of the lines are averaged over all years to obtain a single value for each layer. The slope of the regression line is then the desired constant rate of change per day by transport (black). Note that for the purpose of this plot, the black line has been arbitrarily forced to the same value as the red line at day of year 0 (a) or 151 (b). However, this again has no impact on the parameterization of the "constant change" term or the following derivation of the temperature-dependent term.

a   b
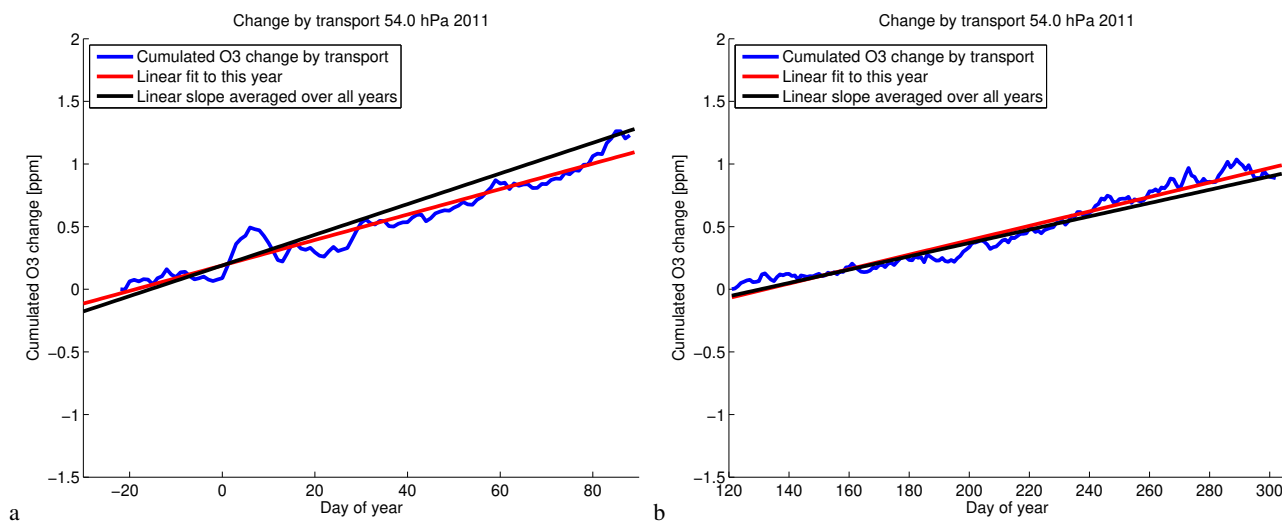
Figure 2. Cumulated vortex-averaged ozone change by transport at 54 hPa for the northern hemispheric winter 2010/2011 (a) and the southern hemispheric winter 2011 (b) (blue), linear fit to the cumulated change (red) and linear slope based on the averaged slope of the fits of all years (black).

Table 2. Fit coefficients (current version)

p [hPa]	69.66111	54.03643	41.59872	31.77399	24.07468	Unit
Constant change term NH	0.1001	0.1224	0.1172	0.1022	0.0786	$\cdot 10^{-7}\text{day}^{-1}$
Constant change term SH	0.1452	0.5316	0.7405	0.8055	0.7902	$\cdot 10^{-8}\text{day}^{-1}$
Temperature-dependent term NH	0.2105	0.2277	0.1862	0.1245	0.0257	$\cdot 10^{-7}\text{K}^{-1}$
Temperature-dependent term SH	0.0541	0.2130	0.2827	0.2958	0.0375	$\cdot 10^{-7}\text{K}^{-1}$

100   The fitted parameters can be found in Table 2. The actual implementation in the ECHAM, ICON-NWP and AFES models is based on an older version of the transport parameterization (using ERA Interim and fewer years). Table 3 shows the fitted parameters for the ECHAM, ICON-NWP and AFES implementation, which are only slightly different.

Table 3. Fit coefficients (used in ECHAM, ICON-NWP and AFES)

p [hPa]	69.66111	54.03643	41.59872	31.77399	24.07468	Unit
Constant change term NH	0.0751	0.0943	0.1010	0.1004	0.0992	$\cdot 10^{-7}\text{day}^{-1}$
Constant change term SH	0.0944	0.4633	0.6919	0.7896	0.7704	$\cdot 10^{-8}\text{day}^{-1}$
Temperature-dependent term NH	0.2162	0.2277	0.1689	0.1049	0.0135	$\cdot 10^{-7}\text{K}^{-1}$
Temperature-dependent term SH	0.1251	0.2423	0.2689	0.2293	-0.0204	$\cdot 10^{-7}\text{K}^{-1}$

3.2 Temperature-dependent term

In addition to the "constant change" term, a temperature-dependent term is included that adds interannual variability to the
transport parameterization. Interannual variability in ozone transport is caused by interannual variability in the Brewer-Dobson
circulation (e.g. Andrews et al., 1987; Fusco and Salby, 1999; Randel et al., 2002; Weber et al., 2003). Vortex temperatures,
the descent in the vortex, and the transport over the vortex edge are all related by the mechanisms of the Brewer-Dobson
circulation. A stronger Brewer-Dobson circulation is related to more adiabatic heating and higher temperatures in the vortex,
which cause more diabatic cooling and descent in the polar vortex.

When assuming a constant zonally averaged radiative equilibrium temperature $\overline{T}_{\mathrm{R}}$, the relationship between zonal mean
temperature at a given date $\overline{T}(0)$ and the downwelling $\overline{w}^*$ (vertical residual velocity in a zonal mean sense in log-pressure
coordinates) of the Brewer-Dobson circulation is approximated by

$$\overline{T}(0) = \overline{T}_{\mathrm{R}} + \exp(-\alpha t)(\overline{T}(-t) - \overline{T}_{\mathrm{R}}) - \int_{-t}^{0} \overline{w}^* S \exp(\alpha t') \, \mathrm{d}t' \tag{2}$$

where $1/\alpha$ is the radiative relaxation time scale (about 1 month), and S is static stability (i.e., the vertical gradient of potential
temperature) (see e.g. Andrews et al., 1987). That is, the temperature difference from the radiative equilibrium temperature
is basically the integral over the downwelling in the past, weighted by an e-folding time of about 1 month. As a further
complication, it has to be considered that $\overline{w}^*$ has to be multiplied by the vertical gradient $\mathrm{d}\chi/\mathrm{d}z$ of a species χ to obtain the
change by transport in this species. This vertical gradient can vary over winter.

We base the temperature-dependent term on an input variable that is readily available from the GCM, and that is the change
in vortex-averaged temperature per time step of the model ΔT_{GCM}. We then try to find a well-working empirical relationship
between this variable and the interannual variation of the change in ozone by transport which is roughly based on the physical
considerations explained above. However, we deliberately choose to simplify our approach as much as possible.

We need a variable $\Delta\mathrm{O}_{3,\mathrm{fit}}$ for the change in ozone and a variable ΔT_{fit} for the change in temperature to obtain a fit for
the temperature-dependent term. For the change in ozone $\Delta\mathrm{O}_{3,\mathrm{fit}}$, we subtract the "constant change" term of the transport
parameterization from the cumulated change of ozone by transport. Note that the "constant change" term is based on the
averaged slope of the changes by transport (and not based on the individual slopes, which would cancel out some of the
interannual variability caused by the Brewer-Dobson circulation). The intercept of the "constant change" term again plays no
role, since it only causes a constant offset which cancels out in the following. This procedure only leaves the changes in ozone
by transport that are different in every year, that is, the interannual variability of ozone by transport. As an example, Figure 3
shows the ozone anomaly $\Delta\mathrm{O}_{3,\mathrm{fit}}$ defined in this way at 54 hPa (layer 2) for the northern hemispheric winter 2010/2011 and
the southern hemispheric winter 2011 (blue).

For the temperature variable ΔT_{fit}, we use the vortex-averaged temperature difference in a layer at a given date compared
to the start date (vortex formation date, see Table 1). This quantity only depends on ERA5. Equation 2 suggests that the
difference in temperature to the start date roughly corresponds to the deviation of the temperature on this day from the radiative
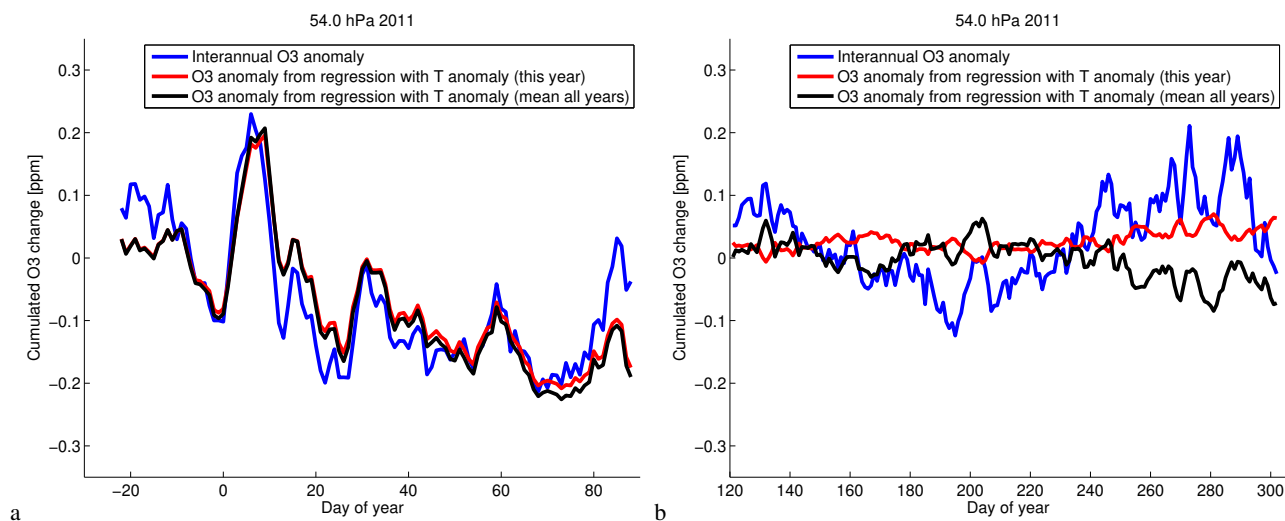
Figure 3. Anomaly of the cumulated vortex-averaged ozone change by transport at 54 hPa for the northern hemispheric winter 2010/2011 (a) and the southern hemispheric winter 2011 (b) (blue, vortex-averaged ozone change by transport after subtraction of the change by transport from the "constant change" term, see Figure 2), the ozone anomaly obtained from a regression with the time series of vortex-averaged temperatures in these years as predictor variables (red), and vortex-averaged temperatures in these years scaled by the mean slope of the regressions of all years (black).

135 equilibrium temperature by the effects of the Brewer-Dobson circulation. According to Equation 2, this would be exactly true when the temperature at the start date would be the radiative equilibrium temperature.

Equation 2 assumes a constant radiative equilibrium temperature. However, the change in temperature from day to day is not only caused by the Brewer-Dobson circulation, but also by the change of the radiative equilibrium temperature with time. For this reason, we now subtract an approximation of the change of the vortex-averaged radiative equilibrium temperature from
140 ΔT_{fit} (the radiative equilibrium temperature is assumed to be identical for any individual year). As a rough approximation for the radiative equilibrium temperature, we simply take the average of the vortex-averaged temperature over all years plus a constant offset. Figure 4 shows the vortex-averaged temperatures for 54 hPa in the northern hemisphere (a) and southern hemisphere (b) for all years (grey lines), and the average over all years (red line). This figure gives us confidence that our approach is feasible: A version of the red line for the average over all years that is shifted down by an constant offset of a few
145 Kelvin (black line) corresponds roughly to the lower envelope of all the grey lines. Assuming that the lower envelope shows situations with a weak Brewer-Dobson circulation where the vortex-averaged temperature approaches the radiative equilibrium temperature, the black curve can be seen as an approximation of the radiative equilibrium temperature. The constant offset of the black line to the red line again plays no role for the results, since it will cancel out in the following. For this reason, we can simply set it to zero again. Note that the approximation of the radiative equilibrium temperature obtained in this way shows the
150 expected temporal evolution, i.e., lower temperatures during polar night.
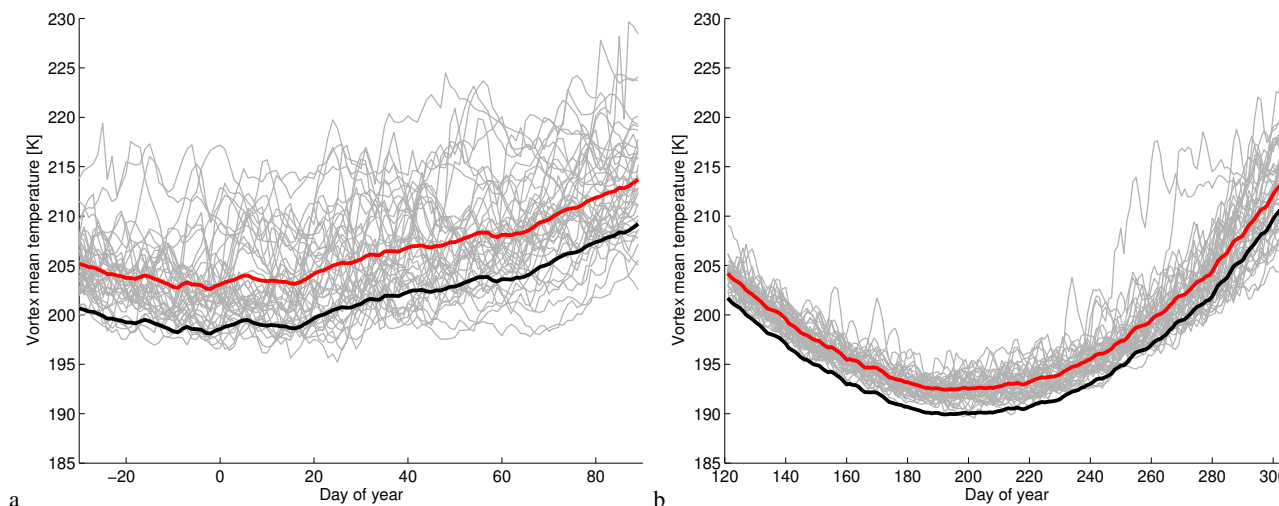
Figure 4. Vortex mean temperatures as a function of day of year for all individual years from 1979/1980 to 2020/2021 (northern hemisphere, a) or 1980–2021 (southern hemisphere, b) based on ERA5 (grey lines), vortex mean temperature averaged over all years (red) and the same curve shifted by $-4.5\,\mathrm{K}$ or $-2.5\,\mathrm{K}$ as an approximation of the lower envelope of the grey lines (black).

Now, we fit a regression line to the relationship of the ozone anomaly $\Delta O_{3,\mathrm{fit}}$ and the temperature anomaly ΔT_{fit} for each individual year (i.e., we obtain a scaling factor that transforms temperature changes into ozone changes). As an example, Figure 3 a shows the temperature anomaly at 54 hPa (layer 2) for the northern hemispheric winter 2010/2011 scaled by the slope of the regression for this year to give the corresponding ozone changes (red). The reasonable agreement between the
155 ozone anomaly (blue) and the scaled temperature anomaly (red) shows that the numerous simplifications in the process of obtaining this empirical parameterization were justified. The method usually works best for the middle layers and the fits are not as good for layer 1 (70 hPa) and 5 (24 hPa), see supplement.

Figure 3 b shows the fit for the southern hemispheric winter 2011. In general, the method works better for the northern hemisphere than for the southern hemisphere. That may partly be explained by the lower magnitude of the interannual changes
160 in the southern hemisphere.

For the parameterization, the slopes of the individual fits are averaged over all years again to obtain a single value for each layer (black). The slope of the regression line has units of ozone change per temperature change. Finally, it is used with the vortex-averaged temperature change per time step ΔT_{GCM} from the GCM to obtain the ozone change of the temperature-dependent term of the transport parameterization. The fitted parameters can be found in Table 2 and Table 3. The change of
165 temperature per time step ΔT_{GCM} has to be corrected for the change of the radiative equilibrium temperature per time step ΔT_{R} before multiplication with the fit parameter. The value that needs to be subtracted for each day of the year can be roughly approximated by the change per day in the vortex-averaged temperature averaged over all years (as shown in Figure 4).

3.3 Final parameterization

The final parameterization for the change of the vortex-averaged ozone by transport in the GCM $\Delta O_{3,\mathrm{GCM}}$ in a given SWIFT
170 layer is

$$\Delta O_{3,\mathrm{GCM}} = c_{\mathrm{const}}\Delta t + c_{\mathrm{T}}(\Delta T_{\mathrm{GCM}} - \Delta T_{\mathrm{R}}) \tag{3}$$

where c_{const} and c_{T} are the fit coefficients (mean slopes) for the "constant change" and temperature-dependent term from
Table 2 or 3. Δt is the time step of the model (in units of days when using the values from Table 2 or 3). ΔT_{GCM} is the change
of temperature within this time step (in units of K), and ΔT_{R} is the same for the change in radiative equilibrium temperature
175 (in units of K).

4 Validation

We use two different methods for validation. First, we validate only the transport term by running a stand-alone version of
the transport parameterization with ERA5 data. Then, we validate a stand-alone version of the complete Polar SWIFT model
(chemistry plus transport parameterization), again driven by ERA5 data.

180 ### 4.1 Stand-alone version of the transport parameterization

First, we calculate the cumulated vortex-averaged ozone change by transport by directly applying Equation 3. Vortex-averaged
temperatures are taken from ERA5. As an example, Figure 5 shows the simulated cumulated change by transport at 54 hPa
(layer 2) for the northern hemispheric winter 2010/2011 and the southern hemispheric winter 2011 (red), compared to the
original transport term from the ATLAS-SWIFT run (blue). To show the contribution of the different terms of Equation 3, the
185 thin grey line shows a simulation with only the "constant change" term, and the thin black line shows a simulation with the
"constant change" and temperature-dependent term, but without subtracting the change of the radiative equilibrium temperature
from the vortex-averaged temperature change.

The difference between the cumulated vortex-averaged ozone change by transport simulated by ATLAS-SWIFT and sim-
ulated by the transport parameterization at the date of vortex breakup is typically about 0.2 ppm in the northern hemisphere
190 (see Figure S28 of the supplement). This is in the order of magnitude of 10 % of the simulated ozone at these dates (see next
section 4.2). The differences in the southern hemisphere are somewhat larger and can reach more than 0.5 ppm and some 10 %
of the simulated ozone at these dates (see Figure S56 of the supplement).

4.2 Complete stand-alone version of SWIFT

The transport parameterization is also validated by runs of a stand-alone version of the complete Polar SWIFT model. The
195 stand-alone version calculates the vortex-averaged ozone mixing ratios as a function of time for the levels that SWIFT is based
on. The model is initialized with values for ozone, HCl, HNO_3 and $ClONO_2$ on the start date. Initial values are taken from
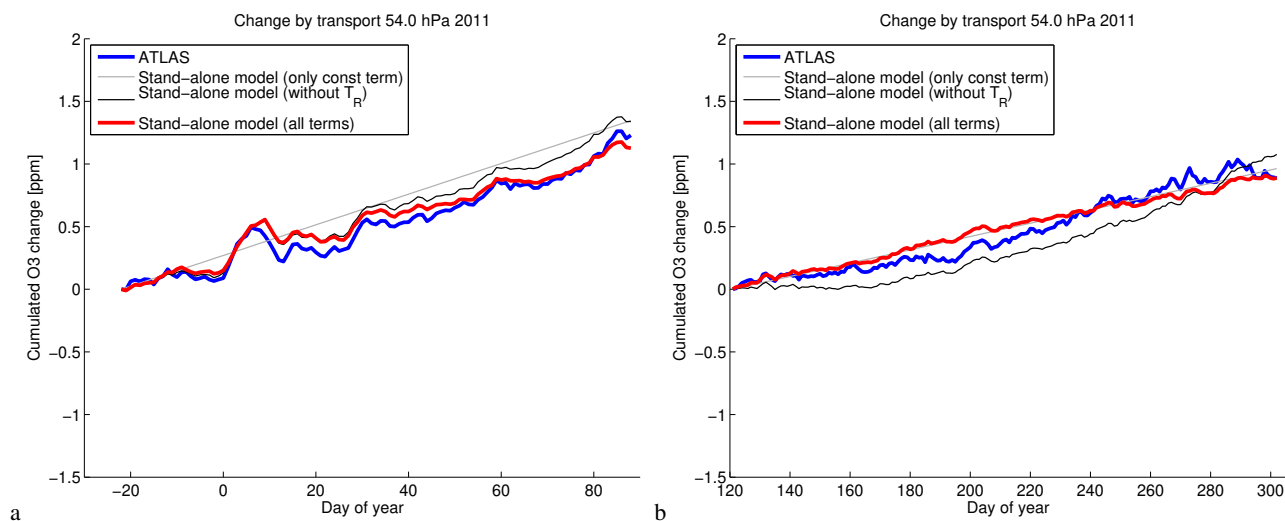
Figure 5. Cumulated vortex-averaged ozone change by transport at 54 hPa for the northern hemispheric winter 2010/2011 (a) and the southern hemispheric winter 2011 (b) as in Figure 2 (blue) and a simulation of the cumulated change by transport by a stand-alone version of the transport parameterization (red). The thin grey line shows a simulation with only the "constant change" term, and the thin black line shows a simulation with the "constant change" and temperature-dependent term, but without subtracting the change of the radiative equilibrium temperature from the vortex-averaged temperature change.

the MLS climatologies (i.e., they are the same for every year). The change of ozone per time step is calculated as the sum of the change by chemistry from the Polar SWIFT model and the change by transport from the transport parameterization. The stand-alone model is driven by meteorological data from ERA5 again. Runs start on 1 November for the northern hemisphere

200 and on 1 May for the southern hemisphere. The transport parametrization is only switched on when a minimum size of the vortex of 15 million km^2 at 54 hPa is exceeded (mainly to account for the fact that the date of vortex formation is usually later than the start date of the model). Chlorine is scaled by EESC in the same way as described above for the ATLAS-SWIFT model. Simulations of the Arctic winters 1979/1980–2020/2021 and the Antarctic winters 1980–2021 are performed. Results are compared to actual measurements of the MLS instrument on a given date for validation.

205 Figure 6 a shows the simulated vortex-averaged ozone at 54 hPa (layer 2) for the date of vortex breakup in the northern hemisphere for different years. The blue line shows the ozone mixing ratios simulated without the transport parameterization (i.e., only the chemistry of the Polar SWIFT model), the brown line shows the ozone mixing ratios simulated with only the "constant change" term of the transport parameterization, and the green line shows the ozone mixing ratios simulated with the full transport parameterization with the "constant change" term and temperature-dependent term. The red line shows

210 corresponding measurements of ozone from the MLS instrument.

The both runs with the transport parameterization agree considerably better with the measurements than the run with only chemistry. However, the difference between the full transport parameterization and the parameterization using only the "constant change" term is relatively small.
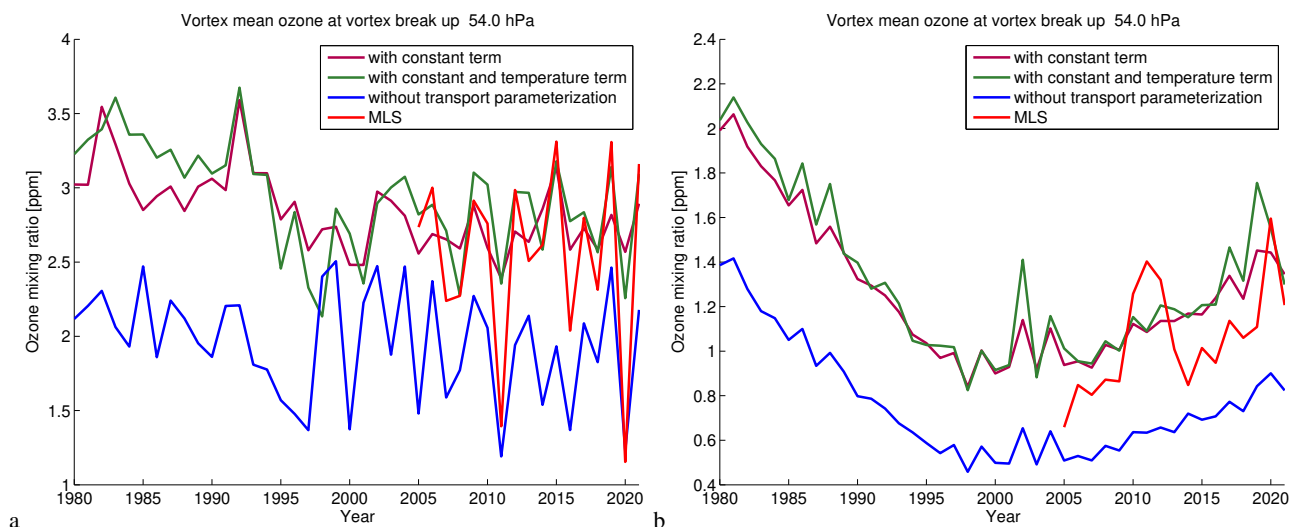
Figure 6. Vortex-averaged ozone at 54 hPa simulated by the stand-alone Polar SWIFT model for the date of vortex breakup in the northern hemisphere (a) and southern hemisphere (b) for different years. Ozone mixing ratios simulated without the transport parameterization (blue), ozone mixing ratios simulated with only the "constant change" term of the transport parameterization (brown), ozone mixing ratios simulated with the full transport parameterization with the "constant change" term and temperature-dependent term (green), and corresponding measurements of ozone from the MLS instrument (red).

Now, we have a look on how well the model results agree with the measurements as a function of the magnitude of the ozone depletion and of the magnitude of the transport in the winter. Figure 7 a shows a scatter plot of the modelled ozone (with the full transport parameterization) versus the observed ozone from MLS (based on the same data as in Figure 6). The model overestimates ozone compared to measurements in winters with low ozone values, that is, in cold winters with large ozone depletion and a weak Brewer-Dobson circulation, while warmer years are simulated relatively well. Note that differences in the simulated ozone are not only caused by differences in chemistry and transport due to the interannual variability in temperatures, but also by systematic differences in the vortex breakup dates. I.e., the vortex breakup is later on average in cold winters with a large ozone depletion. The differences between Polar SWIFT and MLS cannot be explained by the transport parameterization, since they are much larger than the differences of about 0.2 ppm between the transport parameterization and the transport term of ATLAS discussed in the last section 4.1. Hence, the differences between Polar SWIFT and MLS in cold winters must be a deficiency of the chemistry model of Polar SWIFT. However, a discussion of this deficiency is outside the scope of this paper.

Figure 6 b and Figure 7 b show the same for the southern hemisphere. While interannual variability is lower in the southern hemisphere, the model has difficulties to get the mean levels of ozone correct at some levels. That may, e.g., be related to the fact that the assumptions of a linear relationship are less well met in the southern hemisphere (see supplement), or that
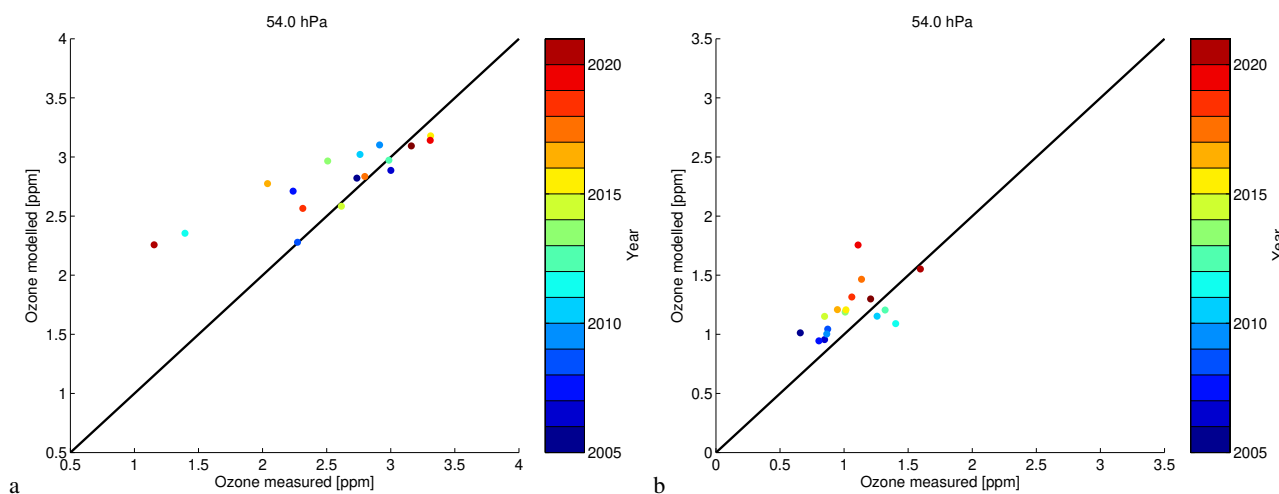
Figure 7. Scatter plots of the modelled ozone (with the full transport parameterization) versus the observed ozone from MLS (based on the same data as in Figure 6).

the transport in the meteorological data from ECMWF in the southern hemisphere is not represented well or that there are
230 deficiencies in the Polar SWIFT chemistry model.

5 Conclusions

We present a transport parameterization for the Polar SWIFT model that simulates the change of vortex-averaged ozone by transport in a fast and simple way without the need for a complex transport scheme in the GCM. In the moment, the transport parameterization and Polar SWIFT are implemented in the ECHAM6, ICON-NWP and AFES4.1 GCMs. We derived the
235 equations for the transport parameterization, fitted the parameterization to the transport simulated in the ATLAS model and validated the parameterization by simulating the original transport term from ATLAS and by comparing the complete Polar SWIFT model to MLS satellite observations. The transport parametrization agrees well with the Lagrangian transport of AT-LAS, with a typical difference of 0.2 ppm in ozone volume mixing ratio at the time of polar vortex break-up. It performs slightly better on the northern hemisphere, than on the southern hemisphere. The constant term of the of the transport parametrization
240 generates a significantly larger contribution to the development of polar ozone over the course of winter than the temperature term.

Code and data availability. The code repository for the ATLAS model can be assessed at https://gitlab.awi.de/iwohltmann/atlas. The scripts used for this manuscript, including the SWIFT stand-alone model, the stand-alone model of the transport parameterization and the start script for ATLAS-SWIFT, are available at doi:10.5281/zenodo.5834222 at Zenodo. MLS data are available at https://disc.gsfc.nasa.gov/datasets?page=1&keywor
245 ECMWF ERA5 data are available at https://cds.climate.copernicus.eu/cdsapp#!/home.

Author contributions. IW developed the transport parameterization, performed the validation runs, wrote the manuscript and produced the figures.

Competing interests. The authors declare that they have no conflict of interest.

Acknowledgements. We thank the MLS Science Team for producing and making public the MLS data. We thank ECMWF for providing ERA5 reanalysis data, generated using Copernicus Climate Change Service Information 2020. Neither the European Commission nor ECMWF is responsible for any use that may be made of the Copernicus Information or Data it contains. Copernicus Climate Change Service (C3S) (2017): ERA5: Fifth generation of ECMWF atmospheric reanalyses of the global climate. Copernicus Climate Change Service Climate Data Store (CDS), 2017–2020.

References

255 Andrews, D. G., Holton, J. R., and Leovy, C. B.: Middle Atmosphere Dynamics, Academic Press, 1987.

Cariolle, D. and Déqué, M.: Southern hemisphere medium-scale waves and total ozone disturbances in a spectral general circulation model, J. Geophys. Res., 91, 10 825–10 846, 1986.

Cariolle, D. and Teyssèdre, H.: A revised linear ozone photochemistry parameterization for use in transport and general circulation models: multi-annual simulations, Atmos. Chem. Phys., 7, 2183–2196, 2007.

260 Enomoto, T., Kuwano-Yoshida, A., Komori, N., and Ohfuchi, W.: Description of AFES 2: Improvements for high-resolution and coupled simulations, in: High resolution numerical modelling of the atmosphere and ocean, chap. 5, pp. 77–97, Springer, New York, https://doi.org/10.1007/978-0-387-49791-4_5, 2008.

Fusco, A. C. and Salby, M. L.: Interannual variations of total ozone and their relationship to variations of planetary wave activity, J. Climate, 12, 1619–1629, 1999.

265 Hersbach, H., Bell, B., Berrisford, P., Hirahara, S., Horányi, A., Muñoz-Sabater, J., Nicolas, J., Peubey, C., Radu, R., Schepers, D., Simmons, A., Soci, C., Abdalla, S., Abellan, X., Balsamo, G., Bechtold, P., Biavati, G., Bidlot, J., Bonavita, M., De Chiara, G., Dahlgren, P., Dee, D., Diamantakis, M., Dragani, R., Flemming, J., Forbes, R., Fuentes, M., Geer, A., Haimberger, L., Healy, S., Hogan, R. J., Hólm, E., Janisková, M., Keeley, S., Laloyaux, P., Lopez, P., Lupu, C., Radnoti, G., de Rosnay, P., Rozum, I., Vamborg, F., Villaume, S., and Thépaut, J.-N.: The ERA5 global reanalysis, Quarterly Journal of the Royal Meteorological Society, 146, 1999–2049, 270 https://doi.org/10.1002/qj.3803, 2020.

Hsu, J. and Prather, M. J.: Stratospheric variability and tropospheric ozone, J. Geophys. Res., 114, D06102, https://doi.org/10.1029/2008JD010942, 2009.

Kuwano-Yoshida, A., Enomoto, T., and Ohfuchi, W.: An improved PDF cloud scheme for climate simulations, Quarterly Journal of the Royal Meteorological Society, 136, 1583–1597, https://doi.org/10.1002/qj.660, 2010.

275 Lait, L. R.: An alternative form for potential vorticity, J. Atmos. Sci., 51, 1754–1759, 1994.

Livesey, N. J., Read, W. G., Wagner, P. A., Froidevaux, L., Lambert, A., Manney, G. L., Valle, L. F. M., Pumphrey, H. C., Santee, M. L., Schwartz, M. J., Wang, S., Fuller, R. A., Jarnot, R. F., Knosp, B. W., Martinez, E., and Lay, R. R.: Earth Observing System (EOS) Aura Microwave Limb Sounder (MLS) Version 4.2x Level 2 and 3 data quality and description document, JPL D-33509 Rev. E, 2020.

McLinden, C. A., Olsen, S. C., Hannegan, B. J., Wild, O., and Prather, M. J.: Stratospheric ozone in 3-D models: a simple chemistry and the 280 cross-tropopause flux, J. Geophys. Res., 105, 14 653–14 665, 2000.

Newman, P. A., Daniel, J. S., Waugh, D. W., and Nash, E. R.: A new formulation of equivalent effective stratospheric chlorine (EESC), Atmos. Chem. Phys., 7, 4537–4552, 2007.

Nowack, P. J., Abraham, N. L., Maycock, A. C., Braesicke, P., Gregory, J. M., Joshi, M. M., Osprey, A., and Pyle, J. A.: A large ozone-circulation feedback and its implications for global warming assessments, Nature Clim. Change, 5, 41–45, 2015.

285 Ohfuchi, W., Nakamura, H., Yoshioka, M. K., Enomoto, T., Takaya, K., Peng, X., Yamane, S., Nishimura, T., Kurihara, Y., and Ninomiya, K.: 10-km Mesh Meso-scale Resolving Simulations of the Global Atmosphere on the Earth Simulator – Preliminary Outcomes of AFES (AGCM for the Earth Simulator) –, Journal of the Earth Simulator, 1, 8–34, 2004.

Randel, W. J., Wu, F., and Stolarski, R.: Changes in column ozone correlated with the stratospheric EP flux, J. Meteorol. Soc. Japan, 80, 849–862, 2002.

290 Rex, M., Salawitch, R. J., Deckelmann, H., von der Gathen, P., Harris, N. R. P., Chipperfield, M. P., Naujokat, B., Reimer, E., Allaart, M., Andersen, S. B., Bevilacqua, R., Braathen, G. O., Claude, H., Davies, J., De Backer, H., Dier, H., Dorokhov, V., Fast, H., Gerding, M., Godin-Beekmann, S., Hoppel, K., Johnson, B., Kyrö, E., Litynska, Z., Moore, D., Nakane, H., Parrondo, M. C., Risley Jr., A. D., Skrivankova, P., Stübi, R., Viatte, P., Yushkov, V., and Zerefos, C.: Arctic winter 2005: Implications for stratospheric ozone loss and climate change, Geophys. Res. Lett., 33, L23808, https://doi.org/10.1029/2006GL026731, 2006.

295 Romanowsky, E., Handorf, D., Jaiser, R., Wohltmann, I., Dorn, W., Ukita, J., Cohen, J., Dethloff, K., and Rex, M.: The role of stratospheric ozone for Arctic-midlatitude linkages, Scientific Reports, 9, 7962, https://doi.org/10.1038/s41598-019-43823-1, 2019.

Thompson, D. W. J. and Solomon, S.: Interpretation of Recent Southern Hemisphere Climate Change, Science, 296, 895–899, 2002.

Weber, M., Dhomse, S., Wittrock, F., Richter, A., Sinnhuber, B.-M., and Burrows, J. P.: Dynamical control of NH and SH winter/spring total ozone from GOME observations in 1995–2002, Geophys. Res. Lett., 30, 1583, https://doi.org/10.1029/2002GL016799, 2003.

300 Wohltmann, I. and Rex, M.: The Lagrangian chemistry and transport model ATLAS: validation of advective transport and mixing, Geosci. Model Dev., 2, 153–173, 2009.

Wohltmann, I., Lehmann, R., and Rex, M.: Update of the Polar SWIFT model for polar stratospheric ozone loss (Polar SWIFT version 2), Geosci. Model Dev., 10, 2671–2689, https://doi.org/10.5194/gmd-10-2671-2017, 2017.

Zängl, G., Reinert, D., Rípodas, P., and Baldauf, M.: The ICON (ICOsahedral Non-hydrostatic) modelling framework of DWD and 305 MPI-M: Description of the non-hydrostatic dynamical core, Quarterly Journal of the Royal Meteorological Society, 141, 563–579, https://doi.org/10.1002/qj.2378, 2015.